Inverse Problems and Imaging doi:10.3934/ipi.2021038

A STABLE NON-ITERATIVE RECONSTRUCTION ALGORITHM FOR THE ACOUSTIC INVERSE BOUNDARY VALUE PROBLEM

Tianyu Yang and Yang Yang*

Department of Computational Mathematics Science and Engineering
Michigan State University
East Lansing, MI 48824, USA

(Communicated by Lauri Oksanen)

Abstract. We present a non-iterative algorithm to reconstruct the isotropic acoustic wave speed from the measurement of the Neumann-to-Dirichlet map. The algorithm is designed based on the boundary control method and involves only computations that are stable. We prove the convergence of the algorithm and present its numerical implementation. The effectiveness of the algorithm is validated on both constant speed and variable speed, with full and partial boundary measurement as well as different levels of noise.

1. **Introduction.** This paper concerns numerical reconstruction of an isotropic wave speed in the inverse boundary value problem (IBVP) for the acoustic wave equation. Specifically, let $T > 0$ be a constant and $\Omega \subset \mathbb{R}^n$ be a bounded domain with smooth boundary $\partial\Omega$. Consider the initial-boundary value problem for the acoustic wave equation:

$$\begin{cases} \partial_t^2 u(t,x) - c^2(x)\Delta u(t,x) &= 0, & \text{in } (0,2T)\times\Omega \\ \partial_\nu u &= f, & \text{on } (0,2T)\times\partial\Omega \\ u(0,x) = \partial_t u(0,x) &= 0 & x \in \Omega. \end{cases} \tag{1}$$

Here $c(x) \in C^\infty(\Omega)$ is a smooth wave speed bounded away from 0 and ∞. Denote the solution by $u(t,x) = u^f(t,x)$.

Given $f \in C_c^\infty((0,2T)\times\partial\Omega)$, the well-posedness of this problem is ensured by the standard theory for second order hyperbolic partial differential equations. Define the Neumann-to-Dirichlet(ND) map:

$$\Lambda_c f := u^f|_{(0,2T)\times\partial\Omega}. \tag{2}$$

The IBVP for the acoustic wave equation aims to recover the wave speed $c(x)$ from the knowledge of the ND map Λ_c.

This inverse problem lies at the core of many imaging technologies. An important example is the *Ultra-Sound Computed Tomography* (USCT). In USCT, a point-like ultrasound source emits an acoustic pulse from a known location outside the tissue. The acoustic wave travels through the tissue and the resulting wave field is recorded by a collection of surrounding ultrasonic transducers. This process is repeated many times for plenty of emitter locations, see Figure 1 for an illustration with M transducers, The goal of USCT is to reconstruct the acoustic wave speed

2020 *Mathematics Subject Classification.* Primary: 35R30; Secondary: 35L05.

Key words and phrases. Acoustic wave equation, inverse boundary value problem, non-iterative reconstruction algorithm, Neumann-to-Dirichlet map, boundary control method.

* Corresponding author: Yang Yang.

everywhere inside the tissue. Similar data acquisition scheme occurs in seismic tomography, where one attempts to recover the underground wave speed to locate oil reservoirs. In the continuous formulation of USCT and seismic tomography, the measurement is the boundary values of the Green's function. However, it is well known [38] that such data is equivalent to knowledge of the ND map Λ_c under mild assumptions.

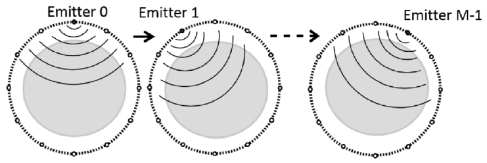

FIGURE 1. Data acquisition scheme in USCT [36]

The IBVP for the acoustic wave equation has been extensively studied in the literature. Among them, Belishev [3] proved that c is uniquely determined using the boundary control (BC) method combined with Tataru's unique continuation result [48]. The result has since been greatly extended to wave equations with lower order terms on Riemannian manifolds with boundary [7, 17, 18, 19, 20, 22, 23, 24, 25, 26, 30, 31, 33, 42, 43, 44]. Stability estimates have been obtained in [1, 2, 8, 9, 14, 34, 37, 45, 46, 47].

The BC method has been numerically implemented to reconstruct the wave speed [5, 6, 41]. The implementation typically involves solving a control problem. This is achieved in [5, 6] using the so-called wave bases, and in [10, 16] using the regularized optimization. In the $1+1$ dimension, a discrete regularization strategy is developed in [28] to recover c from a single pulse-like source. A variant of the BC method has also been applied to detect blockage in networks [12].

In this paper, we develop a BC-based algorithm to reconstruct the wave speed. The derivation is inspired by the theoretical proofs in [34], see also [40]. The algorithm has several favorable features from the computational viewpoint: (1) The algorithm is direct. Conventional computational approaches to recover c relies on minimization of a data misfit functional through iterations. These approaches suffer from local minima, where gradient-descent-based iterations are trapped thus fail to give the true solution to the imaging problem. An example is the cycle-skipping effect in the full waveform inversion. In contrast, a BC-based method solves directly for the solution and involves no iteration. (2) The algorithm converges globally to the true speed. This is again in contrast to iterative algorithms, which converge to the global minimum only when the initial guess is sufficiently accurate. A resulting prospect is that our algorithm could be used to provide a reliable initial guess for iterative methods. (3) The algorithm involves only computations that are stable. Following the idea in [34], one can show that the algorithm is locally Lipschitz stable for a low frequency component of c^{-2}. This is a distinction from the previous BC method in [16]. (4) The algorithm is robust to random noise. The derivation reveals that the ND map is naturally followed by a low-pass filter in the assembly of the connecting operator (see (6)). This filter helps remove high-frequency content in the ND map, leading to robust reconstruction with respect to random noises.

The paper is organized as follows. In Section 2, we derive the reconstruction algorithm and the convergence result using the boundary control theory. In Section 3, we elucidate our implementation of the algorithm using the finite difference scheme. Section 4 is devoted to numerical experiments, where the algorithm is evaluated on both constant speed and variable speed, with full and partial boundary measurement as well as different levels of noise.

2. **Derivation and convergence.** We derive the reconstruction algorithm and show its convergence in this section. Given a function $u(t,x)$, we write $u(t) = u(t,\cdot)$ for the spatial part as a function of x. Introduce the time reversal operator $R : L^2([0,T]\times\partial\Omega) \to L^2([0,T]\times\partial\Omega)$,

$$Ru(t,\cdot) := u(T-t,\cdot), \qquad 0<t<T; \tag{3}$$

and the low-pass filter $J : L^2([0,2T]\times\partial\Omega) \to L^2([0,T]\times\partial\Omega)$

$$Jf(t,\cdot) := \frac{1}{2}\int_t^{2T-t} f(\tau,\cdot)\,d\tau, \qquad 0<t<T. \tag{4}$$

We write $P_T : L^2((0,2T)\times\partial\Omega) \to L^2((0,T)\times\partial\Omega)$ for the orthogonal projection via restriction. Its adjoint operator $P_T^* : L^2((0,T)\times\partial\Omega) \to L^2((0,2T)\times\partial\Omega)$ is the extension by zero from $(0,T)$ to $(0,2T)$. Let $\mathcal{T}_D$ and $\mathcal{T}_N$ be the Dirichlet and Neumann trace operators respectively, that is,

$$\mathcal{T}_D u(t,\cdot) = u(t,\cdot)|_{\partial\Omega}, \qquad \mathcal{T}_N u(t,\cdot) = \partial_\nu u(t,\cdot)|_{\partial\Omega}.$$

Lemma 2.1. *Let u^f be the solution of (1) with $f \in C_c^\infty((0,2T)\times\partial\Omega)$. Suppose $v(t,x) \in C^\infty((0,2T)\times\Omega)$ satisfies the wave equation*

$$(\partial_t^2 - c^2(x)\Delta)v(t,x) = 0, \qquad \text{in } (0,2T)\times\Omega$$

Then

$$(u^f(T), v(T))_{L^2(\Omega,c^{-2}dx)} = (P_T f, J\mathcal{T}_D v)_{L^2((0,T)\times\partial\Omega)} - (P_T(\Lambda_c f), J\mathcal{T}_N v)_{L^2((0,T)\times\partial\Omega)}.$$

where ν is the unit outer normal vector field on $\partial\Omega$.

Proof. Define

$$I(t,s) := (u^f(t), v(s))_{L^2(\Omega,c^{-2}dx)}.$$

We compute

$$\begin{aligned}
&(\partial_t^2 - \partial_s^2)I(t,s)\\
=&(\Delta u^f(t), v(s))_{L^2(\Omega)} - (u^f(t), \Delta v(s))_{L^2(\Omega)}\\
=&(f(t), \mathcal{T}_D v(s))_{L^2(\partial\Omega)} - (\Lambda_c f(t), \mathcal{T}_N v(s))_{L^2(\partial\Omega)},
\end{aligned} \tag{5}$$

where the last equality follows from integration by parts. On the other hand, $I(0,s) = \partial_t I(0,s) = 0$ since $u^f(0,x) = \partial_t u^f(0,x) = 0$. Solve the inhomogeneous 1D wave equation (5) together with these initial conditions to obtain

$$\begin{aligned}
&I(T,T)\\
=&\frac{1}{2}\int_0^T\int_t^{2T-t} \left[(f(t), \mathcal{T}_D v(\sigma))_{L^2(\partial\Omega)} - (\Lambda_c f(t), \mathcal{T}_N v(\sigma))_{L^2(\partial\Omega)}\right] d\sigma dt\\
=&\int_0^T \left[(f(t), \frac{1}{2}\int_t^{2T-t} \mathcal{T}_D v(\sigma)\,d\sigma)_{L^2(\partial\Omega)} - (\Lambda_c f(t), \frac{1}{2}\int_t^{2T-t} \mathcal{T}_N v(\sigma)\,d\sigma)_{L^2(\partial\Omega)}\right] dt\\
=&(P_T f, J\mathcal{T}_D v)_{L^2((0,T)\times\partial\Omega)} - (P_T(\Lambda_c f), J\mathcal{T}_N v)_{L^2((0,T)\times\partial\Omega)}.
\end{aligned}$$

□

We will use the lemma to derive two results. The first is the Blagovescenskii'sidentity. To this end, denote by $\Lambda_{c,T}$ the ND map defined as in (1) (2) yet with $2T$ replaced by T. It can be easily verified from integration by parts that its adjoint operator (with respect to the inner product in $L^2((0,T)\times\partial\Omega)$) is $\Lambda_{c,T}^* = R\Lambda_{c,T}R$ where R is the time reversal operator (3).

Introduce the *connecting operator*

$$K := J\Lambda_c P_T^* - R\Lambda_{c,T}RJP_T^*. \tag{6}$$

The operator K connects inner-products between waves in the interior to measurements on the boundary. It is the principal object of the boundary control method [4]. Moreover, K is a compact operator since $\Lambda_{c,T} : L^2((0,T)\times\partial\Omega) \to H^{2/3}((0,T)\times\partial\Omega)$ is smoothing, see [49].

The Blagoveščenskiĭ's identity we will establish is slightly different from its original form [11]. Instead, it is a reformulation that has been previously used in [10, 39, 15].

Proposition 1. *Let u^f, u^h be the solutions of (1) with Neumann traces $f, h \in L^2((0,T)\times\partial\Omega)$, respectively. Then*

$$(u^f(T), u^h(T))_{L^2(\Omega,c^{-2}dx)} = (f, Kh)_{L^2((0,T)\times\partial\Omega)} = (Kf, h)_{L^2((0,T)\times\partial\Omega)}. \tag{7}$$

In particular if $h = f$, one has

$$\|u^f(T)\|^2_{L^2(\Omega,c^{-2}dx)} = (f, Kf)_{L^2((0,T)\times\partial\Omega)} = (Kf, f)_{L^2((0,T)\times\partial\Omega)}. \tag{8}$$

Proof. We first prove this for $f, h \in C_c^\infty((0,T)\times\partial\Omega)$. Apply Lemma 2.1 to u^f and $v = u^h$ and notice that $\mathcal{T}_D u^h = \Lambda_c P_T^* h$ and $\mathcal{T}_N u^h = P_T^* h$. One has

$$\begin{aligned}
&(u^f(T), u^h(T))_{L^2(\Omega,c^{-2}dx)}\\
=&(P_T f, J\Lambda_c P_T^* h)_{L^2((0,T)\times\partial\Omega)} - (P_T(\Lambda_c f), JP_T^* h)_{L^2((0,T)\times\partial\Omega)}\\
=&(f, J\Lambda_c P_T^* h)_{L^2((0,T)\times\partial\Omega)} - (\Lambda_{c,T} f, JP_T^* h)_{L^2((0,T)\times\partial\Omega)}\\
=&(f, J\Lambda_c P_T^* h)_{L^2((0,T)\times\partial\Omega)} - (f, R\Lambda_{c,T}RJP_T^* h)_{L^2((0,T)\times\partial\Omega)}\\
=&(f, Kh)_{L^2((0,T)\times\partial\Omega)}
\end{aligned}$$

where we have used that $P_T(\Lambda_c f) = \Lambda_{c,T} f$ and that $\Lambda_{c,T}^* = R\Lambda_{c,T}R$ in $L^2((0,T)\times\partial\Omega)$. This establishes the first equality in (7). Interchanging f and h yields the second equality in (7).

For general $f, h \in L^2((0,T)\times\partial\Omega)$, simply notice that K is a continuous operator and that compactly supported smooth functions are dense in L^2. The proof is completed. □

The Blagoveščenskiĭ's identity relates inner products of waves to boundary measurement. Next, we derive an identity that allows computation of inner products between waves and harmonic functions from boundary data. We introduce another operator B that is critical for our reconstruction:

$$B := J\mathcal{T}_D - R\Lambda_{c,T}RJ\mathcal{T}_N. \tag{9}$$

Proposition 2. *Let u^f be the solutions of (1) with Neumann traces $f \in L^2((0,T)\times\partial\Omega)$. For any harmonic function $\phi \in C^\infty(\Omega)$, one has*

$$(u^f(T), \phi)_{L^2(\Omega,c^{-2}dx)} = (f, B\phi)_{L^2((0,T)\times\partial\Omega)}.$$

Proof. We only need to prove this for $f \in C_c^\infty((0,T)\times\partial\Omega)$ by the continuity of B and density of compactly supported functions in L^2. Apply Lemma 2.1 to u^f and $v=\phi$ (since any harmonic function is a time-independent solution of the acoustic wave equation). One has

$$\begin{aligned}(u^f(T),\phi)_{L^2(\Omega,c^{-2}dx)} =&(f, J\mathcal{T}_D\phi)_{L^2((0,T)\times\partial\Omega)} - (P_T(\Lambda_c f), J\mathcal{T}_N\phi)_{L^2((0,T)\times\partial\Omega)}\\ =&(f, J\mathcal{T}_D\phi)_{L^2((0,T)\times\partial\Omega)} - (\Lambda_{c,T} f, J\mathcal{T}_N\phi)_{L^2((0,T)\times\partial\Omega)}\\ =&(f, J\mathcal{T}_D\phi)_{L^2((0,T)\times\partial\Omega)} - (f, R\Lambda_{c,T}RJ\mathcal{T}_N\phi)_{L^2((0,T)\times\partial\Omega)}.\end{aligned}$$

□

Proposition 2 suggests a way to reconstruct the wave speed c from the ND map Λ_c: if for any harmonic function ψ, one can find an explicit sequence f_α such that $u^{f_\alpha}(T)\to\psi$ as $\alpha\to 0$ in $L^2(\Omega,c^{-2}dx)$, then

$$(\psi,\phi)_{L^2(\Omega,c^{-2}dx)} = \lim_{\alpha\to 0}(u^{f_\alpha}(T),\phi)_{L^2(\Omega,c^{-2}dx)} = \lim_{\alpha\to 0}(f_\alpha, B\phi)_{L^2((0,T)\times\partial\Omega)}. \tag{10}$$

The right hand side can be computed from Λ_c, see (9). Thus the integral

$$(\psi,\phi)_{L^2(\Omega,c^{-2}dx)} = \int_\Omega \psi\phi\, c^{-2}(x)\,dx \tag{11}$$

is known for all harmonic functions ψ and ϕ. For any fixed vectors $\xi,\eta\in\mathbb{R}^n$ with $|\xi|=|\eta|$ and $\xi\perp\eta$, choose the complex harmonic functions

$$\psi(x) := e^{\frac{i}{2}(-\xi+i\eta)\cdot x}, \qquad \phi(x) := e^{\frac{i}{2}(-\xi-i\eta)\cdot x}. \tag{12}$$

Then $\psi\phi = e^{i\xi\cdot x}$ and one recovers $\mathcal{F}(c^{-2})$ – the Fourier transform of c^{-2} – by varying ξ. This reconstructs c.

It remains to construct an explicit sequence f_α such that $u^{f_\alpha}(T)\to\psi$ in space $L^2(\Omega,c^{-2}dx)$ as $\alpha\to 0$. We will adopt Tikhonov regularization for the construction. Before that, we record a lemma that will be used in the subsequent analysis.

Lemma 2.2 ([39, Lemma 1])**.** *Let $A: X\to Y$ be a bounded linear operator between two Hilbert spaces X and Y. For any $y\in Y$, let $\alpha>0$ be a constant and $x_\alpha := (A^*A+\alpha)^{-1}A^*y$. Then*

$$Ax_\alpha \to P_{\overline{Ran(A)}}y \qquad \text{as } \alpha\to 0$$

where $P_{\overline{Ran(A)}}y$ denotes the orthogonal projection of y onto the closure of the range of A.

Next, we introduce the *control operator*

$$Wf := u^f(T).$$

where u^f is the solution of (1). According to [32], $W: L^2((0,T)\times\partial\Omega)\to L^2(\Omega)$ is a bounded linear operator. Moreover, Tataru's theorem in [48] implies that W has dense range in $L^2(\Omega)$. It follows from Proposition 1 that $K=W^*W$. It is also easy to verify that $W^*\psi = B\psi$ for any harmonic function ψ.

Proposition 3. *For any harmonic function ψ, the following minimization problem with parameter $\alpha>0$:*

$$f_\alpha := arg\,min_f \|Wf-\psi\|^2_{L^2(\Omega,c^{-2}dx)} + \alpha\|f\|^2_{L^2(0,T)\times\partial\Omega}.$$

has a unique solution $f_\alpha\in L^2((0,T)\times\partial\Omega)$. This solution satisfies the linear equation

$$(K+\alpha)f_\alpha = B\psi. \tag{13}$$

Moreover, $u^{f_\alpha}(T) \to \psi$ *as* $\alpha \to 0$ *in* $L^2(\Omega, c^{-2}dx)$.

Proof. The functional to be minimized is

$$F_\alpha(f) := \|Wf - \psi\|^2_{L^2(\Omega,c^{-2}dx)} + \alpha\|f\|^2_{L^2((0,T)\times\partial\Omega)}.$$

As $W : L^2((0,T)\times\partial\Omega) \to L^2(\Omega)$ is bounded and linear, [27, Theorem 2.11] claims that F_α has a unique minimizer, named f_α, in $L^2((0,T)\times\partial\Omega)$.

To derive the normal equation the minimizer obeys, we rewrite

$$\begin{aligned}
&F_\alpha(f)\\
=&\|u^f(T) - \psi\|^2_{L^2(\Omega,c^{-2}dx)} + \alpha\|f\|^2_{L^2((0,T)\times\partial\Omega)}\\
=&\|u^f(T)\|^2_{L^2(\Omega,c^{-2}dx)} - 2(u^f(T),\psi)_{L^2(\Omega,c^{-2}dx)} + \|\psi\|^2_{L^2(\Omega,c^{-2}dx)} + \alpha\|f\|^2_{L^2(0,T)\times\partial\Omega}\\
=&(f, Kf)_{L^2((0,T)\times\partial\Omega)} - 2(f, B\psi)_{L^2((0,T)\times\partial\Omega)} + \|\psi\|^2_{L^2(\Omega,c^{-2}dx)} + \alpha\|f\|^2_{L^2((0,T)\times\partial\Omega)}\\
=&(f,(K+\alpha)f)_{L^2((0,T)\times\partial\Omega)} - 2(f, B\psi)_{L^2((0,T)\times\partial\Omega)} + \|\psi\|^2_{L^2(\Omega,c^{-2}dx)}
\end{aligned}$$

where we have used Proposition 1 and Proposition 2 in the second but last line. This is a bilinear form of f whose Frechét derivative is

$$F'(f) = 2(K+\alpha)f - 2B\psi.$$

The minimizer satisfies $F'(f_\alpha) = 0$, hence (13).

Finally, since $K = W^*W$ and $B\psi = W^*\psi$ (see the remark before Proposition 3), We conclude from Lemma 2.2 that $Wf_\alpha \to P_{\overline{Ran(W)}}\psi$ in $L^2(\Omega, c^{-2}dx)$ as $\alpha \to 0$. Tataru's theorem [48] claims that the range of W is dense in $L^2(\Omega)$, hence $P_{\overline{Ran(W)}}\psi = \psi$. □

Summarizing the discussion in this section, we have proved global convergence of the following reconstruction algorithm, see Algorithm 1.

Algorithm 1: Non-Iterative Reconstruction Algorithm for Acoustic IBVP.

Input: low-pass filter J, time-reversal operator R, projection operator P_T, ND map Λ_c

Output: wave speed c

1. Assemble the connecting operator $K = J\Lambda_c P_T^* - R\Lambda_{c,T}RJP_T^*$ (see (6)).
2. Assemble the operator $B = J\mathcal{T}_D - R\Lambda_{c,T}RJ\mathcal{T}_N$ (see (9)).
3. Construct the harmonic function $\psi(x) = e^{\frac{i}{2}(-\xi+i\eta)\cdot x}$ (see (12)) and solve the linear system $(K+\alpha)f_\alpha = B\psi$, (see (13)).
4. Construct the harmonic function $\phi(x) := e^{\frac{i}{2}(-\xi-i\eta)\cdot x}$ (see (12)) and compute the Fourier projection
$$\int_\Omega e^{-i\xi\cdot x}c^{-2}(x)\,dx = \lim_{\alpha\to 0}(f_\alpha, B\phi)_{L^2((0,T)\times\partial\Omega)}$$
through the limiting process, (see (10)).
5. Repeat the above steps with various ξ to recover the Fourier transform $\mathcal{F}(c^{-2})$.
6. Invert the Fourier transform to recover c^{-2}, and eventually c.

3. **Algorithm implementation.** In this section, we provide details of our implementation of the algorithm using finite difference discretization.

3.1. **Forward simulation. Computational Domain and Grid.** We take the computational domain $\Omega = [-1,1] \times [-1,1]$, and write $t \in [0,T]$ for the temporal variable and $(x,y) \in \Omega$ for the two spatial coordinates, respectively. Let $0 = t_0 \leq t_1 \leq \cdots \leq t_L = T$ be a partition of the interval $[0,T]$ with uniform spacing $\Delta t = \frac{T}{L}$. Let $-1 = x_0 \leq x_1 \leq \cdots \leq x_I = 1$ be a partition of the interval $[-1,1]$ with uniform spacing $\Delta x = \frac{2}{I}$. Then the temporal grid points are $t_l = l\Delta t \in [0,T]$, $l = 0,1,\ldots,L$. The spatial grid points are $(x_i, y_j) \in \Omega$ with $x_i = x_0 + i\Delta x$ and $y_j = x_0 + j\Delta x$, $i,j = 0,1,\ldots,I$. The total grid size is $(L+1)\times(I+1)\times(I+1)$.

We denote the collection of interior grid points by

$$IGP := \{(t_l, x_i, y_j) : -1 < x_i < 1,\ 1 < y_j < 1,\ i,j = 1,\ldots,I, \quad l = 0,1,\ldots,L\},$$

and the collection of boundary grid points by

$$BGP := \{(t_l, x_i, y_j) : |x_i| = 1,\ |y_j| = 1,\ i,j = 1,\ldots,I, \quad l = 0,1,\ldots,L\}.$$

Let u be the solution to the initial-boundary value problem (1). The values of u on the grid points are denoted by

$$u^l_{ij} := u(t_l, x_i, y_j), \qquad l = 0,1,\ldots,L, \quad i,j = 0,1,\ldots,I.$$

Forward Solver. We solve the inverse boundary value problem (1) by discretizing the acoustic wave equation using the second-order central difference scheme. For the interior grid points, the second order temporal and spatial derivatives are approximated as

$$\partial_t^2 u(t_l, x_i, y_j) \approx \frac{u^{l-1}_{i,j} + u^{l+1}_{i,j} - 2u^l_{i,j}}{\Delta t^2};$$
$$\Delta u(t_l, x_i, y_j) \approx \frac{u^l_{i-1,j} + u^l_{i+1,j} + u^l_{i,j-1} + u^l_{i,j+1} - 4u^l_{i,j}}{\Delta x^2},$$

thus we can update the interior grid points by

$$u^{l+1}_{i,j} = 2u^l_{i,j} - u^{l-1}_{i,j} + c^2(x_i, y_j)\frac{\Delta t^2}{\Delta x^2}[u^l_{i-1,j} + u^l_{i+1,j} + u^l_{i,j-1} + u^l_{i,j+1} - 4u^l_{i,j}],$$

here we set $u^1_{i,j} = u^{-1}_{i,j}$ for the initial condition $\partial_t u|_{t=0} = 0$. For the boundary grid points, the boundary normal derivative (i.e, Neumann data) is computed using the forward/backward finite difference approximation with a second-order accuracy. For instance, for $i = 0$,

$$\partial_\nu u(t_l, x_0, y_j) \approx -\frac{3u^l_{0,j} - 4u^l_{1,j} + u^l_{2,j}}{2\Delta x}.$$

The restriction $\Delta t = \frac{\sqrt{2}}{2c_{max}}\Delta x$ is imposed to fulfill the Courant–Friedrichs–Lewy (CFL) condition. The forward simulation is implemented on the spatial grid with $I = 100$. This grid is finer than the one used in the reconstruction to avoid the inverse crime.

Assembly of the Discrete Neumann-to-Dirichlet Map. The spatial boundary $\partial\Omega$ consists of $4I$ boundary grid points, thus the temporal boundary $[0,T]\times\partial\Omega$ contains $4I(L+1)$ boundary grid points in total. These boundary grid points are ordered in the lexicographical order to form a column vector, that is, a boundary grid point (t_l, x_i, y_j) is ahead of another $(t_{l'}, x_{i'}, y_{j'})$ if and only if (1) $l < l'$; or (2) $l = l'$ and $i < i'$; or (3) $l = l', i = i', j < j'$. In this way, the discretized ND map is a $4I(L+1)\times 4I(L+1)$ square matrix, denoted by $[\Lambda_c] \in \mathbb{R}^{4I(L+1)\times 4I(L+1)}$. In order to find the matrix representation $[\Lambda_c]$, we place a unit source f_{lij} on each boundary grid point $(t_l, x_i, y_j) \in BGP$ as the Neumann data and utilize the forward solver to

obtain the resulting Dirichlet data on all the boundary grid points. Here f_{lij} takes the value 1 on (t_l, x_i, y_j) and 0 on all the other boundary grid points, see Figure 2 for an image of the ND map.

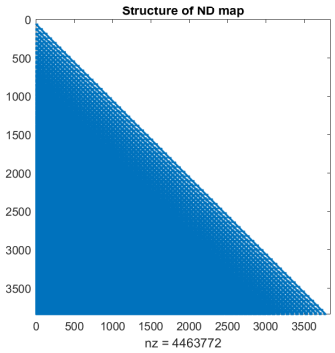

FIGURE 2. The structure of $[\Lambda_c]$ with $I = 15$ and $L = 63$. nz is the number of nonzero elements in the matrix.

3.2. **Reconstruction algorithm. Discretization of the Connecting Operator K.** First, we discretize the operators in the definition of K, see (6). For the filtering operator J, the integral in its definition (4) is discretized using the boundary grid points and trapezoidal rule.

$$\int_{t_l}^{2T-t_l} f(\tau,\cdot)\,d\tau \approx \sum_{k=l}^{L-l-1} \frac{f(t_k,\cdot)+f(t_{k+1},\cdot)}{2}\Delta t.$$

With the arrangement of the boundary grid points in the lexicographical order, the boundary vector consists of $L+1$ small vectors of length $4I$, where each small vector corresponds to the spatial boundary points at the moment $t = t_l, l = 0,\dots,L$. According to the trapezoidal rule, we obtain the matrix representation $[J] \in \mathbb{R}^{2I(K+1)\times 4I(K+1)}$. It can be partitioned into $\lceil \frac{L+1}{2} \rceil \times (L+1)$ blocks, where $\lceil \frac{L+1}{2} \rceil$ denotes the smallest integer no smaller than $\frac{L+1}{2}$, see Figure 3. Each block is a $4I \times 4I$ identity matrix $[I]$ multiplied by the coefficients of the trapezoidal integration formula. Specifically, if L is odd,

$$[J] = \frac{\Delta t}{2}\begin{pmatrix} [I] & 2[I] & 2[I] & \dots & \dots & \dots & \dots & 2[I] & 2[I] & [I] \\ & [I] & 2[I] & \dots & \dots & \dots & \dots & 2[I] & [I] & \\ & & \ddots & \ddots & & & \iddots & \iddots & & \\ & & & [I] & 2[I] & 2[I] & [I] & & & \\ & & & & [I] & [I] & & & & \end{pmatrix},$$

If L is even,

$$[J] = \frac{\Delta t}{2}\begin{pmatrix} [I] & 2[I] & 2[I] & \dots & \dots & \dots & 2[I] & 2[I] & [I] \\ & [I] & 2[I] & \dots & \dots & \dots & 2[I] & [I] & \\ & & \ddots & \ddots & & \iddots & \iddots & & \\ & & & [I] & 2[I] & [I] & & & \\ & & & & [O] & & & & \end{pmatrix},$$

where $[O]$ is the $4I \times 4I$ zero matrix.

Likewise, the time-reversal operator R defined in (3) and the restriction operator P_T are discretized to obtain their discrete counterparts $[R] \in \mathbb{R}^{2I(L+1)\times 2I(L+1)}$ and $[P_T] \in \mathbb{R}^{2I(L+1)\times 4I(L+1)}$. Thanks to the lexicographical order of the boundary grid points, these matrices have block structures as well: $[R]$ is a square anti-diagonal block matrix where the blocks are $4I\times 4I$ identity matrices, and $[P_T]$ is a rectangular matrix with 1 on the main diagonal:

$$[P_T] = \begin{pmatrix} [I]_{[4I\lceil \frac{L+1}{2} \rceil]\times[4I\lceil \frac{L+1}{2} \rceil]} & [O] \end{pmatrix}, [R] = \begin{pmatrix} & & [I] \\ & \iddots & \\ [I] & & \end{pmatrix}$$

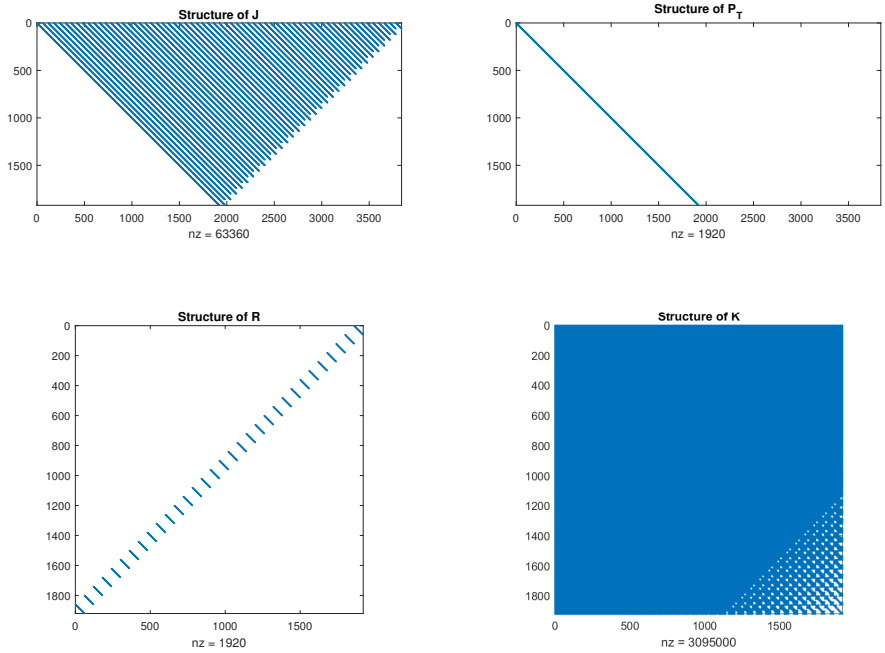

FIGURE 3. The structure of $[J], [P_T], [R], [K]$ with $I = 15$ and $L = 63$. nz is the number of nonzero elements in the matrix.

The discretized adjoint $[P_T^*]$ is taken to be $[P_T]^t$, the transpose of $[P_T]$. Finally, the discretized K is the following matrix product, according to (6):

$$[K] = [J][\Lambda_c][P_T]^t - [R][\Lambda_{c,T}][R][J][P_T]^t \qquad \in \mathbb{R}^{2I(L+1)\times 2I(L+1)}.$$

In general, $[K]$ is not a sparse matrix. An image of $[K]$ is illustrated in Figure 3. Since K is a compact operator (see the remark below (6)), $[K]$ is ill-conditioned. Its singular values are plotted in Figure 4.

Discretization of the Operator B. With the aforementioned discretized operators, the discretized B is naturally the following matrix product, according to (9):

$$[B] = [J][\mathcal{T}_D] - [R][\Lambda_{c,T}][R][J][\mathcal{T}_N] \qquad \in \mathbb{R}^{2I(L+1)\times 4I(L+1)}.$$

Here the matrices $[\mathcal{T}_D], [\mathcal{T}_N] \in \mathbb{R}^{4I(L+1)\times 4I(L+1)}$ are of large size, thus their storage takes up lots of memory. However, observing that the operator B is applied only to

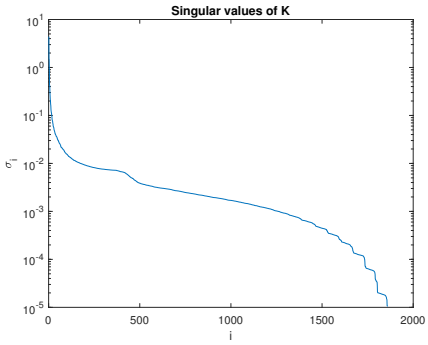

FIGURE 4. The singular values of $[K]$ with $I = 15, L = 63$. $[K]$ has 60 zero singular values.

harmonic functions which are time-independent, we can reduce the cost of memory by first computing these matrices at a specific time, then shifting them to other times. Since the harmonic functions in our numerical experiments are all handcrafted, we can also compute their boundary values from the analytic expressions.

Solving for f_α. The next step is to solve for $[f_\alpha]$ from the discretized version of (13):

$$([K] + \alpha)[f_\alpha] = [B][\psi|_{\partial\Omega}]. \tag{14}$$

Here $[f_\alpha]$ is the discretized version of f_α in (13); ψ is an arbitrary harmonic function and $[\psi|_{\partial\Omega}] \in \mathbb{R}^{4I(L+1)\times 1}$ denotes the vectorized boundary restriction $\psi|_{\partial\Omega}$. Both $[f_\alpha]$ and $\psi|_{\partial\Omega}$ are in the lexicographical order as before. Since $[K]$ has zero singular values, we solve (13) with Tikhonov regularization. Specifically, the equation that we solve is

$$([K]^t[K] + \alpha)[f_\alpha] = [K]^t[B][\psi|_{\partial\Omega}] \tag{15}$$

where $[K]^t$ is the transpose of $[K]$.

Solving for $[c^{-2}]$. The last step is to solve for $[c^{-2}]$. In the proof of Algorithm 1, this is accomplished by constructing appropriate complex exponential harmonic functions (12) and inverting the Fourier transform. Nonetheless, such harmonic functions are not suitable for numerical implementation: they tend to blow up due to their exponential growth in certain directions.

We instead exploit the fundamental solutions method (FSM) to construct harmonic functions. This method, first proposed by Kupradze [29], features ease of numerical implementation. Its applicability for general elliptic boundary value problems has been investigated in [13], see also the review paper [21]. In FSM, one uses harmonic functions of the form

$$\sum_{j=1}^{n} a_j \Phi(|x - x^{(j)}|) \tag{16}$$

Here a_j are real scalars and Φ is (up to a constant factor) the fundamental solution of the Laplace operator: $\Phi(r) = \log r$ for $n = 2$ and $\Phi(r) = \frac{1}{r}$ for $n \geq 3$. These functions are harmonic except at the singularities $x^{(j)}$, which are chosen to be outside the computational domain. It has been shown [35] that an arbitrary 2D

function which is harmonic inside the unit disk and continuous up to the boundary can be approximated to any prescribed accuracy using functions of the form (16).

We proceed to discretize the identity (10). On the right-hand side of (10), we fix a small $\alpha > 0$ and approximate the boundary integral over $[0,T] \times \partial\Omega$ using the trapezoidal rule:

$$(f_\alpha, B\phi)_{L^2((0,T)\times\partial\Omega)} \approx \sum_{j=1}^{4I(L+1)} w_j [f_\alpha]_j [B\phi|_{\partial\Omega}]_j \tag{17}$$

where $[f_\alpha]$ has been obtained from the previous step, and $[B\phi|_{\partial\Omega}]$ is computed from the matrix multiplication $[B\phi|_{\partial\Omega}] = [B][\phi|_{\partial\Omega}]$. On the left-hand side of (10), we approximate the interior integral over Ω by successively applying the trapezoidal rule first to y and then to x. If we write $w = (\frac{1}{2}, 1, \ldots, 1, \frac{1}{2}) \in \mathbb{R}^{I+1}$ for the coefficient vector of the trapezoidal rule, then

$$\begin{aligned} (\psi, \phi)_{L^2(\Omega, c^{-2}dx)} &= \int_{-1}^{1}\int_{-1}^{1} \psi(x,y)\phi(x,y)c^{-2}(x,y)\,dxdy \\ &\approx \sum_{j,k=0}^{I} w_j w_k \psi(x_j,y_k)\phi(x_j,y_k)c^{-2}(x_j,y_k)(\Delta x)^2. \end{aligned} \tag{18}$$

Finally, we equating (17) and (18) and inserting various harmonic functions of the form (16). This gives rise to a system of linear equations on the unknowns $c^{-2}(x_j, y_k)$, $j,k = 0,1,\ldots,I$. If the number of harmonic functions is small, the linear system will be under-determined. In this circumstance, we employ Tikhonov regularization to solve for the regularized unknowns.

4. Numerical experiments.

We validate the reconstruction algorithm in this section with several numerical examples. All the numerical experiments are conducted on a Windows 10 laptop with Intel Core i7-9750H 2.6GHz CPU and 16GB RAM.

For the forward simulation, we employ a computational grid of size $(2L+1) \times 101 \times 101$ to generate the ND map. For the inverse problem, we re-sample the ND map on a coarser grid of size $(L+1) \times 51 \times 51$ and implement Algorithm 1 there to avoid the inverse crime. Here the value of L depends on the choice of c.

We construct the following harmonic functions in view of (16):

$$\begin{aligned} \phi^{(1)} &= \ln((x-2.3)^2 + (y-2.2)^2), & \phi^{(2)} &= \ln((x+2.5)^2 + (y-2.1)^2), \\ \phi^{(3)} &= \ln((x-2.7)^2 + (y+1.9)^2), & \phi^{(4)} &= \ln((x+1.5)^2 + (y+2.5)^2), \\ \phi^{(5)} &= \ln((x+1.2)^2 + (y+2.5)^2), & \phi^{(6)} &= 1. \end{aligned}$$

We denote the vector space generated by the products of these harmonic functions by S_6, that is,

$$S_6 := \operatorname{span}\{\phi^{(i)}\phi^{(j)} : i,j = 1,\ldots,6\}.$$

If c^{-2} is in the vector space S_6, we can decompose

$$c^{-2} = \sum_{1\le i\le j\le 6} c_{ij}\phi^{(i)}\phi^{(j)}.$$

Take the inner product $(\cdot,\cdot)_{L^2(\Omega)}$ with $\phi^{(k)}\phi^{(l)}$ respectively, $k,l=1,\dots,6$, to obtain the following linear system

$$\mathbf{A}\cdot\begin{bmatrix} c_{11}\\ c_{12}\\ \vdots\\ c_{66}\end{bmatrix}=\begin{bmatrix} (c^{-2},{\phi^{(1)}}^2)_{L^2(\Omega)}\\ (c^{-2},\phi^{(1)}\phi^{(2)})_{L^2(\Omega)}\\ \vdots\\ (c^{-2},{\phi^{(7)}}^2)_{L^2(\Omega)}\end{bmatrix}. \tag{19}$$

where the 21×21 coefficient matrix $\mathbf{A}$ is

$$\begin{bmatrix} ({\phi^{(1)}}^2,{\phi^{(1)}}^2)_{L^2(\Omega)} & ({\phi^{(1)}}^2,\phi^{(1)}\phi^{(2)})_{L^2(\Omega)} & \dots & ({\phi^{(1)}}^2,{\phi^{(6)}}^2)_{L^2(\Omega)}\\ (\phi^{(1)}\phi^{(2)},{\phi^{(1)}}^2)_{L^2(\Omega)} & (\phi^{(1)}\phi^{(2)},\phi^{(1)}\phi^{(2)})_{L^2(\Omega)} & \dots & (\phi^{(1)}\phi^{(2)},{\phi^{(6)}}^2)_{L^2(\Omega)}\\ \vdots & \vdots & \ddots & \vdots\\ ({\phi^{(6)}}^2,{\phi^{(1)}}^2)_{L^2(\Omega)} & ({\phi^{(6)}}^2,\phi^{(1)}\phi^{(2)})_{L^2(\Omega)} & \dots & ({\phi^{(6)}}^2,{\phi^{(6)}}^2)_{L^2(\Omega)}\end{bmatrix}$$

The coefficient matrix on the left-hand side can be directly computed, and the components of the vector on the right-hand side are exactly the inner products on the left hand side of (18). We then solve the discretized version of this linear system to obtain the coefficients c_{ij}.

If c^{-2} is not in the vector space S_6, the inner products on the right hand side of (19) project c^{-2} orthogonally onto S_6. Solving the linear system just yields such orthogonal projection. As the products of harmonic functions are dense in $L^2(\Omega)$, one can expect the orthogonal projection to better approximate c^{-2} with increased number of harmonic functions $\phi^{(j)}$.

Experiment 1: $c\equiv 1$ and $c^{-2}\in S_6$.

We test the reconstruction of a constant speed $c\equiv 1$ in this experiment. Notice that $c^{-2}\equiv 1\in S_6$ since $\phi^{(6)}=1$. The reconstructed images along with the errors are illustrated in Figure 5, in the presence of 0%, 5% and 50% of Gaussian random noises with zero mean and unit variance respectively. We observe that addition of the random noise has almost negligible impact on the reconstructed images. This is because in the definition (6) of K, the ND map is followed by the low-pass filter J, which tends to smoothing out the random noise. As a justification, we also test the impact of non-random noise on the reconstruction. We re-run the code with constant noise 0.01, 0.02, and 0.05 added to the ND map. In this case, the filter fails to smooth out the noise, and the reconstructions are significantly compromised. The resulting errors in the discretized connecting operator $[K]$ are shown in Table 1.

Random Noise	Relative Frobenius Error
10%	3.74%
20%	7.51%
50%	18.80%
Constant Noise	**Relative Frobenius Error**
0.01	119.01%
0.02	238.01%
0.05	595.03%

TABLE 1. Impact of random and constant noises on $[K]$.

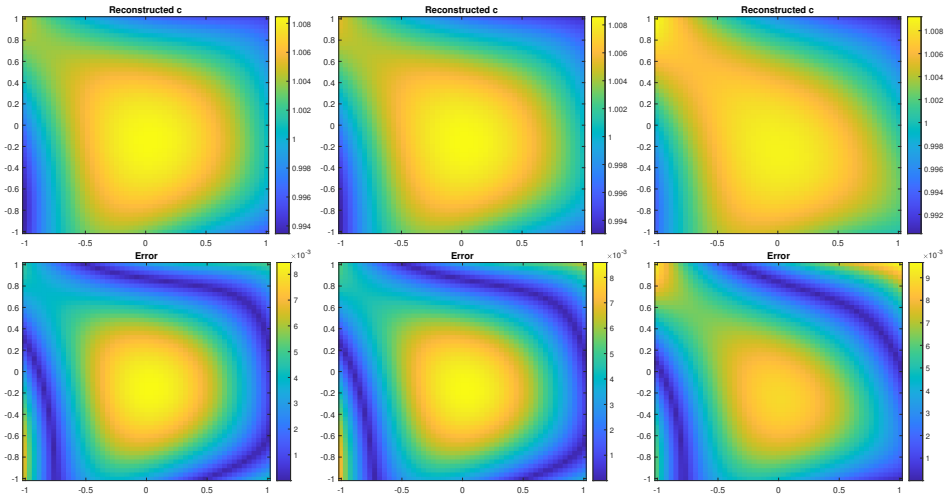

FIGURE 5. Reconstructions of the constant speed $c = 1$. Top row: reconstructed c. Bottom row: error between the reconstruction and the ground truth. First column: 0% noise; the relative L^2-error is 0.4769%. Second column: 5% noise; the relative L^2-error is 0.4873%. Third column: 50% noise; the relative L^2-error is 0.5454%. Grid: $283 \times 51 \times 51$, $I = 50, L = 282$.

Experiment 2: c is variable and $c^{-2} \in S_6$.

Next, we test the algorithm for a variable speed c with $c^{-2} \in S_6$. The random Gaussian noise is fixed to be 5% in this experiment. The ground-truth speed is

$$c^{-2} = \sum_{i=1}^{6} \frac{i}{10} \phi^{(i)},$$

see the leftmost of Figure 6. We perform the reconstructions with the first 2, 4, and 6 harmonic functions $\phi^{(i)}$, respectively, in order to show the improvement of the image quality as the number of basis functions increases. We observe that the reconstruction is increasingly accurate as the number of harmonic functions increases, see the numerical validation in Figure 7.

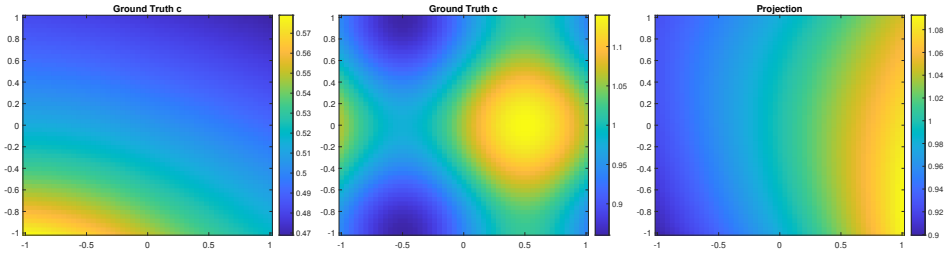

FIGURE 6. Left: the variable speed $c^{-2} = \sum_{i=1}^{6} \frac{i}{10} \phi^{(i)}$. Middle: the variable speed $c(x, y) = 1 + 0.08 \sin \pi x + 0.06 \cos \pi y$. Right: orthogonal projection of $c(x, y) = 1 + 0.08 \sin \pi x + 0.06 \cos \pi y$ on S_6.

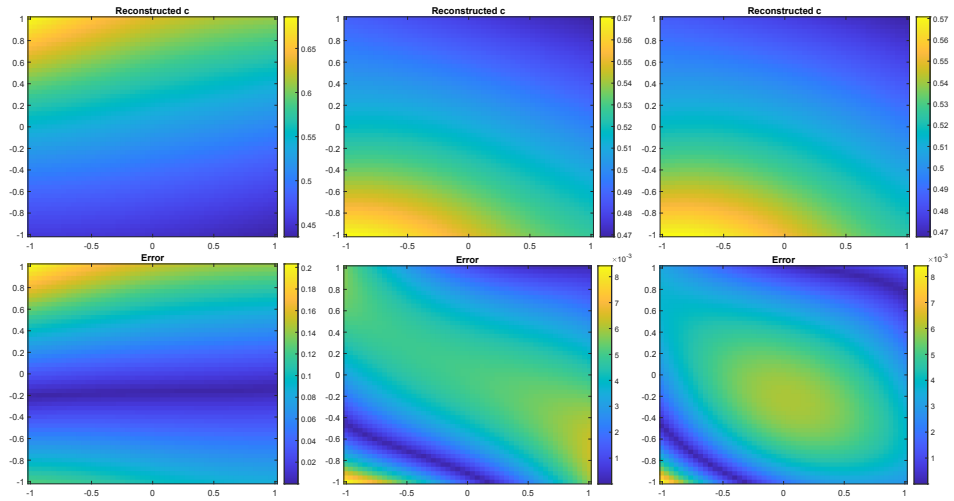

FIGURE 7. Reconstructions of the variable speed $c^{-2} = \sum_{i=1}^{6} \frac{i}{10}\phi^{(i)}$. Top row: reconstructed c. Bottom row: error between the reconstruction and the ground truth. First column: First 2 harmonic functions; the relative L^2-error is 15.6987%. Second column: First 4 harmonic functions; the relative L^2-error is 0.7939%. Third column: All 6 harmonic functions; the relative L^2-error is 0.7907%. Grid: $323 \times 51 \times 51$, $I = 50, L = 163$.

Experiment 3: c is variable and $c^{-2} \notin S_6$.

Next, we test the ability of the algorithm in recovering a variable speed c with $c^{-2} \notin S_6$. The speed in use is

$$c(x, y) = 1 + 0.08 \sin \pi x + 0.06 \cos \pi y,$$

as is illustrated in Figure 6. The reconstructions with the first 2, 4, and 6 harmonic functions $\phi^{(i)}$ are shown in Figure 8. In this case, we cannot expect to reconstruct the exact discrete version of c^{-2}. Instead, what the algorithm yields is the L^2-orthogonal projection of c^{-2} onto the subspace S_6. This is due to the use of Tikhonov regularization when solving for $[c^{-2}]$. See the numerical validation in Figure 8.

Experiment 4: partial data.

We test the algorithm with only partial knowledge of the ND map. We use the constant speed $c = 1$, although the variable speed in Experiment 3 works almost equally well. Recall that the computational domain Ω is a square with four sides $x = \pm 1$ and $y = \pm 1$. We remove the knowledge of the ND map from the three sides $y = -1$, $x = 1$, $y = 1$ one after another. The reconstructions are shown in Figure 9, where the algorithm performs quite well. This is due to the large stoppage T we choose. No noise is imposed in this experiment.

Experiment 5: c is discontinuous

This case is not covered by the theory, as Algorithm 1 is derived under the assumption that c is smooth. We still test it anyway. The wave speed is

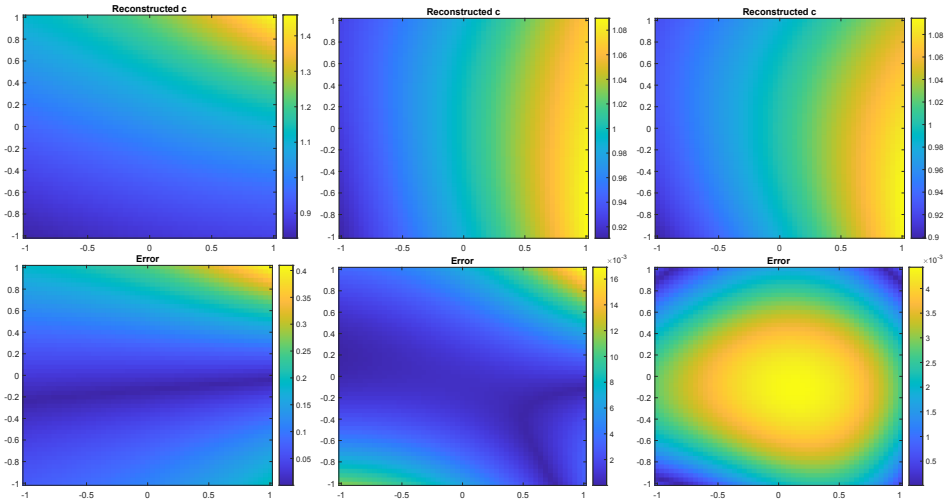

FIGURE 8. Reconstructions of the variable speed $c(x,y) = 1 + 0.08\sin\pi x + 0.06\cos\pi y$. Top row: reconstructed c. Bottom row: error between the reconstruction and the orthogonal projection of the ground truth. First column: First 2 harmonic functions; the relative L^2-error is 12.3535%. Second column: First 4 harmonic functions; the relative L^2-error is 0.4139%. Third column: All 6 harmonic functions; the relative L^2-error is 0.3104%. Grid: $323 \times 51 \times 51$, $I = 50, L = 322$.

$$c(x,y) = \begin{cases} 1 & (x,y) \in [-0.5,0.5]^2, \\ 0.5 & (x,y) \in \Omega \setminus [-0.5,0.5]^2, \end{cases}$$

see Figure 10. Again, the algorithm is able to reconstruct only the orthogonal projection of the discontinuous speed on S_6. However, this project is smooth and does not look like the original discontinuous speed, see Figure 11. No noise is imposed in this experiment.

Acknowledgments. The authors are grateful to Dr. Lauri Oksanen for introducing them to the problem and for communicating many references. The authors would also like to thank the anonymous referee for many valuable comments, and for suggesting several references regarding the fundamental solutions method. The research of T. Yang and Y. Yang is partially supported by the NSF grant DMS-1715178, DMS-2006881, and startup fund from Michigan State University.

REFERENCES

[1] I. B. Aïcha, Stability estimate for a hyperbolic inverse problem with time-dependent coefficient, *Inverse Problems*, **31** (2015), 125010, 21 pp.

[2] G. Bao and H. Zhang, Sensitivity analysis of an inverse problem for the wave equation with caustics, *J. Amer. Math. Soc.*, **27** (2014), 953–981.

[3] M. I. Belishev, An approach to multidimensional inverse problems for the wave equation, in *Soviet Math. Dokl.*, **36** (1988), 481–484.

[4] M. I. Belishev, Recent progress in the boundary control method, *Inverse Problems*, **23** (2007), R1–R67.

[5] M. I. Belishev and V. Y. Gotlib, Dynamical variant of the BC-method: Theory and numerical testing, *J. Inverse Ill-Posed Probl.*, **7** (1999), 221–240.

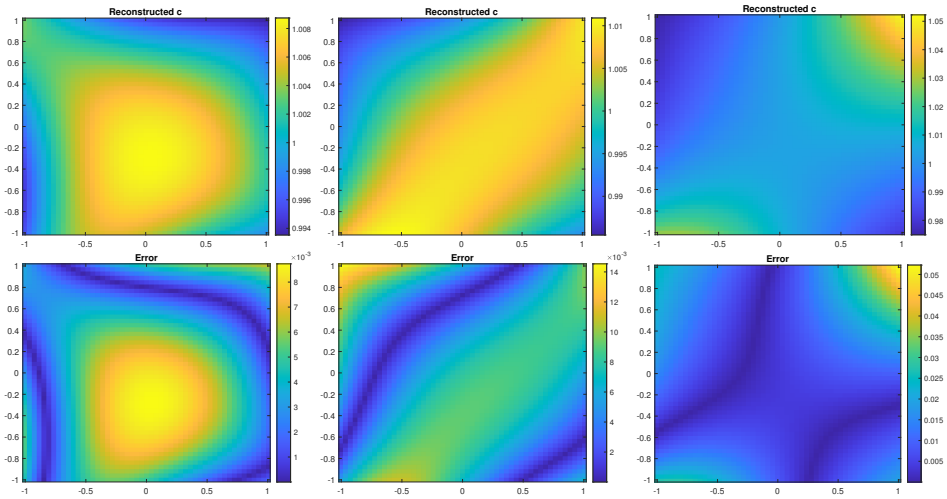

FIGURE 9. Top row: reconstructed c. Bottom row: error between the reconstruction and the ground truth. First column: no data on $y = -1$; the relative L^2-error is 0.4954%. Second column: no data on $y = -1$ and $x = 1$; the relative L^2-error is 0.6583%. Third column: no data on $y = \pm 1$ and $x = 1$; the relative L^2-error is 1.2518%. Grid: $283 \times 51 \times 51$, $I = 50, L = 282$.

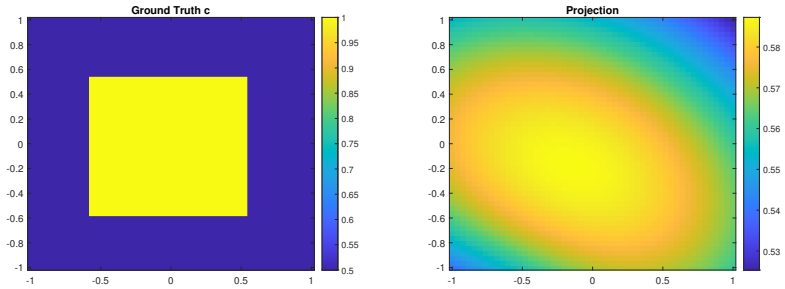

FIGURE 10. The ground truth speed c and its projection.

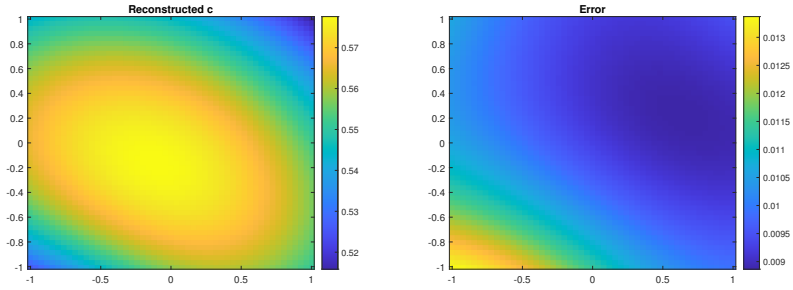

FIGURE 11. Left: reconstructed c. Right: error between the reconstruction and the orthogonal projection of the ground truth. The relative L^2 error is 1.7289%. Grid: $283 \times 51 \times 51$, $I = 50, L = 282$.

[6] M. I. Belishev, I. B. Ivanov, I. V. Kubyshkin and V. S. Semenov, Numerical testing in determination of sound speed from a part of boundary by the BC-method, *J. Inverse Ill-Posed Probl.*, **24** (2016), 159–180.

[7] M. I. Belishev and Y. V. Kuryiev, To the reconstruction of a Riemannian manifold via its spectral data (BC–method), *Comm. Partial Differential Equations*, **17** (1992), 767–804.

[8] M. Bellassoued and I. B. Aïcha, Stable determination outside a cloaking region of two time-dependent coefficients in an hyperbolic equation from Dirichlet to Neumann map, *J. Math. Anal. Appl.*, **449** (2017), 46–76.

[9] M. Bellassoued and D. Dos Santos Ferreira, Stability estimates for the anisotropic wave equation from the Dirichlet-to-Neumann map, *Inverse Probl. Imaging*, **5** (2011), 745–773.

[10] K. Bingham, Y. Kurylev, M. Lassas and S. Siltanen, Iterative time-reversal control for inverse problems, *Inverse Probl. Imaging*, **2** (2008), 63–81.

[11] A. S. Blagoveščenskiĭ, The inverse problem in the theory of seismic wave propagation, in *Spectral Theory and Wave Processes*, Springer, **1** (1966), 68–81.

[12] E. Blåsten, F. Zouari, M. Louati and M. S. Ghidaoui, Blockage detection in networks: The area reconstruction method, *Math. Eng.*, **1** (2019), 849–880. arXiv:1909.05497.

[13] A. Bogomolny, Fundamental solutions method for elliptic boundary value problems, *SIAM J. Numer. Anal.*, **22** (1985), 644–669.

[14] R. Bosi, Y. Kurylev and M. Lassas, Reconstruction and stability in Gel'fand's inverse interior spectral problem, arXiv preprint, arXiv:1702.07937.

[15] M. V. de Hoop, P. Kepley and L. Oksanen, An exact redatuming procedure for the inverse boundary value problem for the wave equation, *SIAM J. Appl. Math.*, **78** (2018), 171–192.

[16] M. V. de Hoop, P. Kepley and L. Oksanen, Recovery of a smooth metric via wave field and coordinate transformation reconstruction, *SIAM J. Appl. Math.*, **78** (2018), 1931–1953.

[17] G. Eskin, A new approach to hyperbolic inverse problems, *Inverse Problems*, **22** (2006), 815–831.

[18] G. Eskin, Inverse hyperbolic problems with time-dependent coefficients, *Comm. Partial Differential Equations*, **32** (2007), 1737–1758.

[19] G. Eskin, Inverse problems for the Schrödinger equations with time-dependent electromagnetic potentials and the Aharonov–Bohm effect, *J. Math. Phys.*, **49** (2008), 022105, 18 pp.

[20] G. Eskin, Inverse problems for general second order hyperbolic equations with time-dependent coefficients, *Bull. Math. Sci.*, **7** (2017), 247–307.

[21] G. Fairweather and A. Karageorghis, The method of fundamental solutions for elliptic boundary value problems, *Adv. Comput. Math.*, **9** (1998), 69–95.

[22] A. Feizmohammadi and Y. Kian, Recovery of non-smooth coefficients appearing in anisotropic wave equations, *SIAM J. Math. Anal.*, **51** (2019), 4953–4976. arXiv:1903.08118.

[23] G. Hu and Y. Kian, Determination of singular time-dependent coefficients for wave equations from full and partial data, *Inverse Probl. Imaging* **12** (2018), 745–772. arXiv:1706.07212.

[24] V. Isakov and Z. Sun, Stability estimates for hyperbolic inverse problems with local boundary data, *Inverse Problems*, **8** (1992), 193–206.

[25] Y. Kian, Recovery of time-dependent damping coefficients and potentials appearing in wave equations from partial data, *SIAM J. Math. Anal.*, **48** (2016), 4021–4046.

[26] Y. Kian and L. Oksanen, Recovery of time-dependent coefficient on Riemannian manifold for hyperbolic equations, *Int. Math. Res. Not. IMRN*, **2019** (2019), 5087–5126.

[27] A. Kirsch, *An Introduction to the Mathematical Theory of Inverse Problems*, vol. 120, Springer Science & Business Media, 2011.

[28] J. Korpela, M. Lassas and L. Oksanen, Discrete regularization and convergence of the inverse problem for $1 + 1$ dimensional wave equation, *Inverse Probl. Imaging*, **13** (2019), 575–596.

[29] V. D. Kupradze, On the approximate solution of problems in mathematical physics, *(Russian) Uspehi Mat.*, **22** (1967), 59–107.

[30] Y. V. Kurylev and M. Lassas, Hyperbolic inverse problem with data on a part of the boundary, in *UAB-GIT International Conference on Differential Equations and Mathematical Physics*, American Mathematical Society, **16** (2000), 259–272.

[31] Y. Kurylev, L. Oksanen and G. P. Paternain, Inverse problems for the connection laplacian, *J. Differential Geom.*, **110** (2018), 457–494.

[32] I. Lasiecka and R. Triggiani, Regularity theory of hyperbolic equations with non-homogeneous Neumann boundary conditions. II. General boundary data, *J. Differential Equations*, **94** (1991), 112–164.

[33] M. Lassas and L. Oksanen, Inverse problem for the Riemannian wave equation with Dirichlet data and Neumann data on disjoint sets, *Duke Math. J.*, **163** (2014), 1071–1103.
[34] S. Liu and L. Oksanen, A Lipschitz stable reconstruction formula for the inverse problem for the wave equation, *Trans. Amer. Math. Soc.*, **368** (2016), 319–335.
[35] R. Mathon and R. L. Johnston, The approximate solution of elliptic boundary-value problems by fundamental solutions, *SIAM J. Numer. Anal.*, **14** (1977), 638–650.
[36] T. P. Matthews and M. A. Anastasio, Joint reconstruction of the initial pressure and speed of sound distributions from combined photoacoustic and ultrasound tomography measurements, *Inverse Problems*, **33** (2017), 124002, 24 pp.
[37] C. Montalto, Stable determination of a simple metric, a covector field and a potential from the hyperbolic Dirichlet-to-Neumann map, *Comm. Partial Differential Equations*, **39** (2014), 120–145.
[38] A. I. Nachman, Reconstructions from boundary measurements, *Ann. of Math.*, **128** (1988), 531–576.
[39] L. Oksanen, Solving an inverse obstacle problem for the wave equation by using the boundary control method, *Inverse Problems*, **29** (2013), 035004, 12 pp.
[40] L. N. Pestov, On reconstruction of the speed of sound from a part of boundary, *J. Inverse Ill-Posed Probl.*, **7** (1999), 481–486.
[41] L. Pestov, V. Bolgova and O. Kazarina, Numerical recovering of a density by the BC-method, *Inverse Probl. Imaging*, **4** (2010), 703–712.
[42] A. G. Ramm and Rakesh, Property C and an inverse problem for a hyperbolic equation, *J. Math. Anal. Appl.*, **156** (1991), 209–219.
[43] R. Salazar, Determination of time-dependent coefficients for a hyperbolic inverse problem, *Inverse Problems*, **29** (2013), 095015, 17 pp.
[44] P. D. Stefanov, Uniqueness of the multi-dimensional inverse scattering problem for time dependent potentials, *Math. Z.*, **201** (1989), 541–559.
[45] P. Stefanov and G. Uhlmann, Stability estimates for the hyperbolic Dirichlet to Neumann map in anisotropic media, *J. Funct. Anal.*, **154** (1998), 330–358.
[46] P. Stefanov and G. Uhlmann, Stable determination of generic simple metrics from the hyperbolic Dirichlet-to-Neumann map, *Int. Math. Res. Not.*, **2005** (2005), 1047–1061.
[47] P. Stefanov and Y. Yang, The inverse problem for the Dirichlet-to-Neumann map on Lorentzian manifolds, *Anal. PDE*, **11** (2018), 1381–1414.
[48] D. Tataru, Unique continuation for solutions to PDE's; between Hörmander's theorem and Holmgren's theorem, *Comm. Partial Differential Equations*, **20** (1995), 855–884.
[49] D. Tataru, On the regularity of boundary traces for the wave equation, *Ann. Scuola Norm. Sup. Pisa Cl. Sci.*, **26** (1998), 185–206.

Received January 2021; revised March 2021.

E-mail address: yangti27@msu.edu
E-mail address: yangy5@msu.edu